Journal of Intelligent Transportation Systems, 12(4):159–167, 2008

ISSN: 1547-2450 print / 1547-2442 online
DOI: 10.1080/15472450802448138

Taylor & Francis
Taylor & Francis Group

Integration of Steering Angle Sensor with Global Positioning System and Micro-Electro-Mechanical Systems Inertial Measurement Unit for Vehicular Positioning

JIANCHEN GAO,[1] MARK PETOVELLO,[2] and M. ELIZABETH CANNON[3]

[1]QUALCOMM, San Diego, California, USA
[2]Department of Geomatics Engineering, Schulich School of Engineering, University of Calgary, Calgary, Alberta, Canada
[3]Geomatics Engineering, Schulich School of Engineering, University of Calgary, Calgary, Alberta, Canada

The concept of using the steering angle sensor to enhance positioning accuracy during Global Positioning System (GPS) outages is the focus of this article. This development of a GPS Micro-Electro-Mechanical Systems Inertial Measurement Unit (MEMS IMU) steering angle sensor vehicular positioning system is discussed in detail including the error dynamics and measurement models as well as integration strategy. With postmission and real-time field tests, the benefits in terms of the horizontal positioning accuracy after integrating the steering angle sensors are analyzed. With respect to GPS/MEMS IMU integrated system, the percentage improvement gained when including the steering angle sensor is over 50% for the open-sky test when GPS outages are simulated, and about 30% for the real-time tests conducted in the suburban and pseudourban environments.

Keywords Steering Angle Sensor; MEMS IMU; GPS; Sensor Integration

With the increase in demand for safe and reliable vehicle operation, significant attention is being given to intelligent vehicle systems whereby the positioning accuracy and system redundancy have crucial impacts on performance. A GPS/MEMS IMU integrated system is commonly used for these systems (Dissanayake et al., 2001; Godha, 2006); however, the performance of a low cost MEMS IMU degrades quickly over even short GPS satellite outages which can cause significant error drifts.

Augmenting a GPS/MEMS IMU system with onboard sensors built into modern vehicles provides the most direct and cost-effective aiding sources. To date, research on GPS/MEMS IMU/Onboard vehicle sensor integration has mainly focused on wheel speed sensors and low cost gyros (Bonnifait, 2003; Kubo et al., 1999, Harvey, 1998, Stephen, 2000); however, to improve accuracy and redundancy, numerous other sensors are being employed in advanced intelligent vehicle systems. Significant work has also been done to integrate GPS with other lower cost sensors to aid positioning and/or attitude determination. These sensors have ranged from the use of a compass, tilt meter, and fiber-optic gyro for vehicle pitch and azimuth estimation (Harvey, 1998), to the integration of GPS with an on-board odometer in an antilock braking system (ABS) as well as a gyro for positioning in urban areas (Stephen, 2000). Wheel speed sensors are fundamental components of an ABS, which is standard equipment on most vehicles (Hay, 2005). The integration of a wheel speed sensor with GPS/INS (Inertial Navigation System) has been extensively studied. Kubo and colleagues (1999) implemented a GPS/INS/Wheel speed sensor integrated system in the wander angle frame for land-vehicle positioning, and proposed an algorithm to calibrate two tilt angles (azimuth and pitch) between the wheel speed sensor and the IMU body frame. Bonnifait (2003) developed an inexpensive vehicle localization system by using GPS and ABS sensors (four odometers), which are available on

Address correspondence to Jianchen Gao, 12906 Camel Creek Rd #9, San Diego, CA 92130, USA. E-mail: jianchengao@gmail.com

most modern cars. It showed that wheel speed sensors could also provide positioning information at several meters accuracy by integrating with GPS.

As a key device in modern vehicles, the steering angle sensor plays an important role in the vehicle stability and in autonomous control systems. The use of the steering angle sensor, as discussed in the literature, is mainly used in the context of an automatic vehicle steering system (Carlson, 2003; Bevly, 2001); however, how to make use of the steering angle sensor to enhance the positioning accuracy during GPS outages has not been fully investigated and is the focus of this article.

This article aims to develop a vehicular positioning system suited for an intelligent and autonomous vehicle control system with centimeter level positioning accuracy in open sky areas with good GPS availability. To this end, standalone GPS with pseudorange only cannot meet this positioning accuracy. In related research, the integration of GPS with an odometer, compass, and/or gyroscope is more cost effective than using a MEMS IMU; however, an odometer is susceptible to slippage, which is a main limitation for achieving high accuracy. Furthermore, this kind of low-cost navigation system cannot provide orientation information, such as pitch and roll, that is commonly used in autonomous and intelligent vehicle control systems.

Herein, the development of a GPS/MEMS IMU/Steering angle sensor vehicular positioning system is discussed in detail including the integration strategy, error dynamics, and measurement models. Raw GPS measurements (pseudorange, Doppler, and carrier phase) are used in a double difference approach so that centimeter level accuracy can be achieved when GPS is fully available and integer ambiguities are resolved. A tight coupling strategy is implemented for the integration of GPS, the MEMS IMU and the steering angle sensor. To compensate for the measurement error in the steering angle sensor, the scale factor and bias are estimated by a centralized Kalman filter. The benefits gained from the steering angle sensor are investigated in terms of the horizontal position accuracy achieved in open sky tests with data processed through post-mission and real-time testing conducted in suburban and pseudo-urban areas. A highly accurate independent reference trajectory is generated by using a GPS/tactical-grade HG1700 IMU system for the open-sky tests and a GPS/navigation-grade CIMU integrated system for the real-time tests.

A description of the steering angle sensor, the integration strategy, as well as the error dynamics and measurement models of the GPS/MEMS IMU/Steering Angle Sensor (SAS) are discussed in the second section. The tests are described, and the results analyzed to investigate the benefits gained from the steering angle sensor in the third section. Conclusions are given in the fourth section.

STEERING ANGLE SENSOR AND ITS INTEGRATION WITH GPS AND MEMS IMU

As illustrated by Figure 1, the steering angle sensor measures the front tire turning angle with respect to the neutral position.

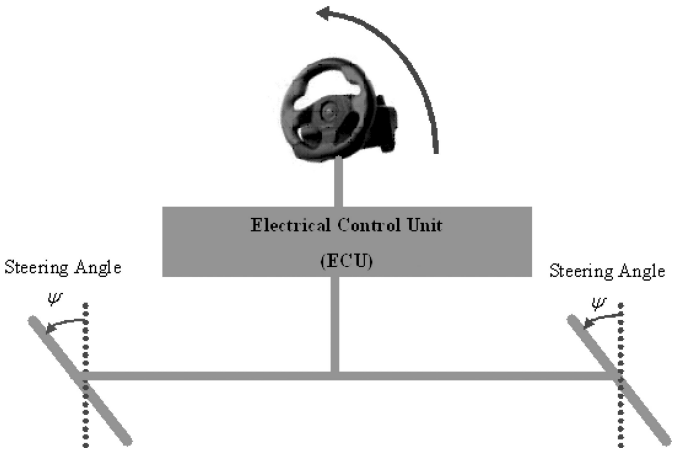

Figure 1 Steering Angle (Gao, 2007).

Through an electrical control unit, the operation of the steering wheel is transformed into steering angle information with respect to the neutral position by using a constant scale factor provided by the manufacturer. Because the transformation implemented by the electrical control unit is nonlinear by nature, a constant scale factor as used herein is only an approximation of the real situation.

The basic concept of integrating a steering angle sensor is to compute the estimated steering angle from the integrated velocity in the vehicle frame, and then to employ the steering angle measurement to update the centralized Kalman filter. The vehicle frame (v frame) refers to the vehicle's body frame, and represents the orientation of the vehicle. The origin is the vehicle's center of gravity. The X-axis points towards the right side of the vehicle and the Y-axis points towards the forward direction of the vehicle's motion. The Z-axis is orthogonal to the X and Y axes to complete a right-handed frame. Figure 2 shows the integration strategy of the GPS/MEMS IMU/Steering Angle Sensor (SAS) system. The sensors are integrated using a tight coupling strategy at each epoch to obtain a globally optimal solution using one centralized Kalman filter. For the equipment used, the IMU data rate is 100 Hz, and its mechanization equation output rate is set to 10 Hz. The position, velocity and attitude information of the integrated system are given by implementing the mechanization equation of the IMU in the Earth-Centered, Earth-Fixed (ECEF) frame. The GPS measurements used herein are double differenced carrier phase, double differenced Doppler, and double differenced pseudorange at a 1 Hz rate.

Due to some of the nonlinear characteristics in the Electrical Control Unit (ECU) and the steering actuator, the transformation between the steering wheel angle and the vehicle tire angle is nonlinear. To adapt to the variation of this transformation, the scale factor of the steering angle sensor is augmented into error states of the Kalman filter. A constant bias exists in the steering angle sensor measurement. If left uncompensated, it will degrade the steering angle sensor measurement accuracy, and, therefore, needs to be estimated by the centralized Kalman filter. The external update to the centralized Kalman filter, through

GPS and the steering angle sensor, facilitates the estimation of error states including position errors, velocity errors, misalignment angles, the scale factor and bias of the steering angle sensor as well as accelerometer and gyro biases. When the GPS carrier phase ambiguities are not resolved as integers, the float double differenced ambiguities are augmented and estimated in the centralized Kalman filter. Integer ambiguities are resolved using the LAMBDA method (Teunissen and Kleusberg, 1996).

The implemented centralized Kalman filter works in a closed loop mode. In one manner, the GPS provides an external aid to limit the INS drift error and estimates the steering angle sensor errors when GPS is available. During GPS outages, the steering angle sensor will continue to update the centralized Kalman filter and bridge the GPS data gap. In another way, the estimated error states feedback to the integrated solution as well as the IMU and steering angle sensor measurements. With feedback information, the integrated position, velocity, and attitude angles can be corrected by the estimated error states of position, velocity, and the misalignment angles. Also, the estimated accelerometer and gyro biases, as well as augmented steering angle sensor error states, can rectify the IMU and steering angle sensor measurements.

The error dynamics and measurement models used in the Kalman filter are derived to include the integration of the steering angle sensor. In its dynamics model, the scale factor and bias of the steering angle sensor are augmented into the error state vector of the GPS/INS centralized Kalman filter. The scale factor and steering angle sensor bias are all modeled as random constants and the dynamics model is therefore expressed by Eq. (1).

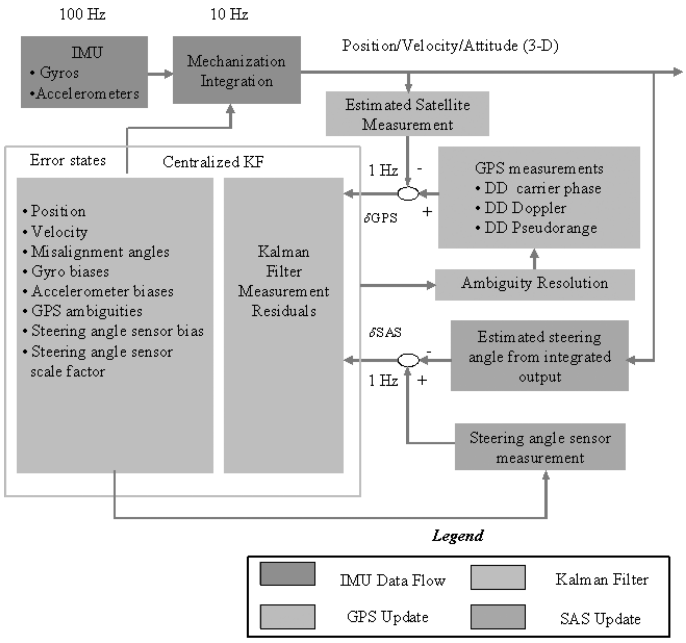

Figure 2 GPS/INS/SAS Integration Strategy.

$$\begin{bmatrix} \delta\dot{r} \\ \delta\dot{v} \\ \dot{\varepsilon}^e \\ \delta\dot{b}^b \\ \delta\dot{d}^b \\ \Delta\nabla\dot{N} \\ \delta\dot{S}_{SAS} \\ \delta\dot{d}_{SAS} \end{bmatrix} = \begin{bmatrix} 0 & I & 0 & 0 & 0 & 0 & 0 & 0 \\ N^e & -2\Omega_{ie}^e & -F^e & R_b^e & 0 & 0 & 0 & 0 \\ 0 & 0 & -\Omega_{ie}^e & 0 & R_b^e & 0 & 0 & 0 \\ 0 & 0 & 0 & -diag(\alpha_i) & 0 & 0 & 0 & 0 \\ 0 & 0 & 0 & 0 & -diag(\beta_i) & 0 & 0 & 0 \\ 0 & 0 & 0 & 0 & 0 & 0 & 0 & 0 \\ 0 & 0 & 0 & 0 & 0 & 0 & 0 & 0 \\ 0 & 0 & 0 & 0 & 0 & 0 & 0 & 0 \end{bmatrix} \begin{bmatrix} \delta r \\ \delta v \\ \varepsilon^e \\ \delta b^b \\ \delta d^b \\ \Delta\nabla N \\ \delta S_{SAS} \\ \delta d_{SAS} \end{bmatrix} + \begin{bmatrix} 0 & 0 & 0 & 0 \\ R_b^e & 0 & 0 & 0 \\ 0 & R_b^e & 0 & 0 \\ 0 & 0 & I & 0 \\ 0 & 0 & 0 & I \\ 0 & 0 & 0 & 0 \\ 0 & 0 & 0 & 0 \\ 0 & 0 & 0 & 0 \end{bmatrix} \begin{bmatrix} w_f \\ w_w \\ w_b \\ w_d \end{bmatrix} = F_{GPS/INS/SAS}\delta x + G_{GPS/INS/SAS}w \tag{1}$$

where a superscript "e" refers to a parameter in the ECEF frame, a superscript "b" refers to a parameter in the body frame, δr^e is the position error vector, δv^e is the velocity error vector, ε^e is the misalignment angle error vector, δb^b is the vector of the accelerometer bias errors, δd^b is the vector of the gyro bias errors, $\Delta\nabla N$ is the vector of double difference carrier phase ambiguities, w_f is the accelerometer noise, w_w is the gyro noise, $diag(\alpha_i)$ is the diagonal matrix of the time constant reciprocals for the accelerometer bias model, $diag(\beta_i)$ is the diagonal matrix of the time constant reciprocals for the gyro bias models, w_b is the driving noise for the accelerometer biases, w_d is the driving noise for the gyro biases, R_b^e is the direction

cosine matrix between body frame and ECEF frame, F^e is the skew-symmetric matrix of specific force, N^e is the tensor of the gravity gradients, Ω^e_{ie} is the skew-symmetric matrix of the Earth rotation with respect to the e frame, δS_{SAS} is the error state of the steering angle sensor scale factor, $\delta d_{SAS}$is the error state of the steering angle sensor bias, $F_{GPS/INS/SAS}$ is the dynamics matrix of the GPS/INS/SAS integration strategy, and $G_{GPS/INS/SAS}$ is the shaping matrix of the GPS/INS/SAS integrated system.

It is noted that the MEMS sensors are generally highly sensitive to temperature variations, which means that the temperature sensitivity must be accommodated, either in the system model (above) or somewhere else. For this work, tests were conducted under approximate isothermal conditions in order to evaluate the performance of the system under ideal temperature conditions. Further work would be necessary to accommodate temperature variations.

Assuming the sideslip of the front tire is zero, the steering angle can be estimated from the velocity in the vehicle frame. The measurement model for the steering angle sensor is given by

$$S_{SAS}\psi - d_{SAS} = -\tan^{-1}\left(\frac{v^v_x}{v^v_y}\right) + w_m \tag{2}$$

where S_{SAS} is the scale factor of the steering angle sensor, d_{SAS} is the bias of the steering angle sensor, ψ is the steering angle sensor measurement, and w_m is measurement noise. v^x and v^y are the integrated velocity expressed in the x and y axes of the vehicle frame, respectively.

To comply with the Kalman filter assumptions, the measurement noise in the steering angle sensor is assumed to be Gaussian white noise with zero mean and uncorrelated over time. Gaussian white noise is a good approximation of many real-world situations. Because it is difficult to find a reference for evaluating the measurement accuracy of the steering angle sensor, the steering angle measurement noise can be either determined empirically through testing various scenarios in the Kalman filter or indirectly estimated from the derived steering angle from other sensor measurements with known accuracy by using variance propagation theory (e.g., Gao, 2007).

The negative sign on the right hand side of Eq. (2), which represents the estimated steering angle from the velocity in the vehicle frame, is due to the definition of the vehicle frame as Right-Front-Up, while a positive steering angle corresponds to a left turn which is contrary in sign to the value calculated from the estimated velocity. The velocity in Eq. (2) is defined in the vehicle frame, which is obtained by transforming the velocity from the ECEF frame, as shown in Eq. (3),

$$v^v = R^v_b\left(R^e_b\right)^T v^e \tag{3}$$

where R^v_b is the direction cosine matrix between body frame and ECEF frame.

The measurement model indicates that the steering angle is observed from the velocity. In static mode, the steering angle sensor cannot provide the external update to the Kalman filter as the estimated steering angle derived from the velocity becomes undetermined. In kinematic mode, however, the steering angle sensor can constrain the velocity drift, and consequently limit the positioning error during partial and complete GPS outages.

The design matrix, H_{SAS}, used in the Kalman filter for measurement update is derived by the perturbation of measurement model. The following intermediate variables can be defined, namely,

$$C_{v^e} = R^v_b(R^e_b)^T$$

$$C_{\varepsilon^e} = R^v_b(R^e_b)^T v^E$$

$$C_{H\delta v^e} = \left[\frac{C_{v^e}(2,1)v^v_x - C_{v^e}(1,1)v^v_y}{(v^v_x)^2+(v^v_y)^2}\ \frac{C_{v^e}(2,2)v^v_x - C_{v^e}(1,2)v^v_y}{(v^v_x)^2+(v^v_y)^2}\right.$$

$$\left.\frac{C_{v^e}(2,3)v^v_x - C_{v^e}(1,3)v^v_y}{(v^v_x)^2+(v^v_y)^2}\right],$$

and

$$C_{H\varepsilon^e} = \left[\frac{C_{\varepsilon^e}(2,1)v^v_x - C_{\varepsilon^e}(1,1)v^v_y}{(v^v_x)^2+(v^v_y)^2}\ \frac{C_{\varepsilon^e}(2,2)v^v_x - C_{\varepsilon^e}(1,2)v^v_y}{(v^v_x)^2+(v^v_y)^2}\right.$$

$$\left.\frac{C_{\varepsilon^e}(2,3)v^v_x - C_{\varepsilon^e}(1,3)v^v_y}{(v^v_x)^2+(v^v_y)^2}\right]$$

where C_{v^e} is the coefficient of the perturbation of velocity in the v frame with respect to the velocity error state, C_{ε^e} is the coefficient of perturbation of the velocity in the v frame with respect to misalignment angles, and $C_{v^e}(i, j)$ represents the element of C_{v^e} matrix at the *i-th* row and *j-th* column. $C_{\varepsilon^e}(i, j)$ represents the element of C_{ε^e} matrix at the *i-th* row and *j-th* column.

Without losing generality, the design matrix for the steering angle measurement update is, therefore, summarized in Eq. (4):

$$H_{SAS} = \left[\, O_{1\times3}\ C_{H\delta v^e}\ C_{H\varepsilon^e}\ O_{1\times3}\ O_{1\times3}\ O_{1\times AR}\ -\psi\ 1.0\,\right] \tag{4}$$

TESTS, RESULTS, AND ANALYSIS

The field tests included an open-sky kinematic test processed in postmission and real-time tests in suburban and pseudourban areas. The pseudourban area approximates an urban canyon environment but with overall lower masking angles and with severe masking conditions occurring for significantly shorter durations than in a real urban canyon (Petovello, 2003). Each test ran for several minutes in static mode for IMU alignment and then 20–30 minutes in kinematic mode.

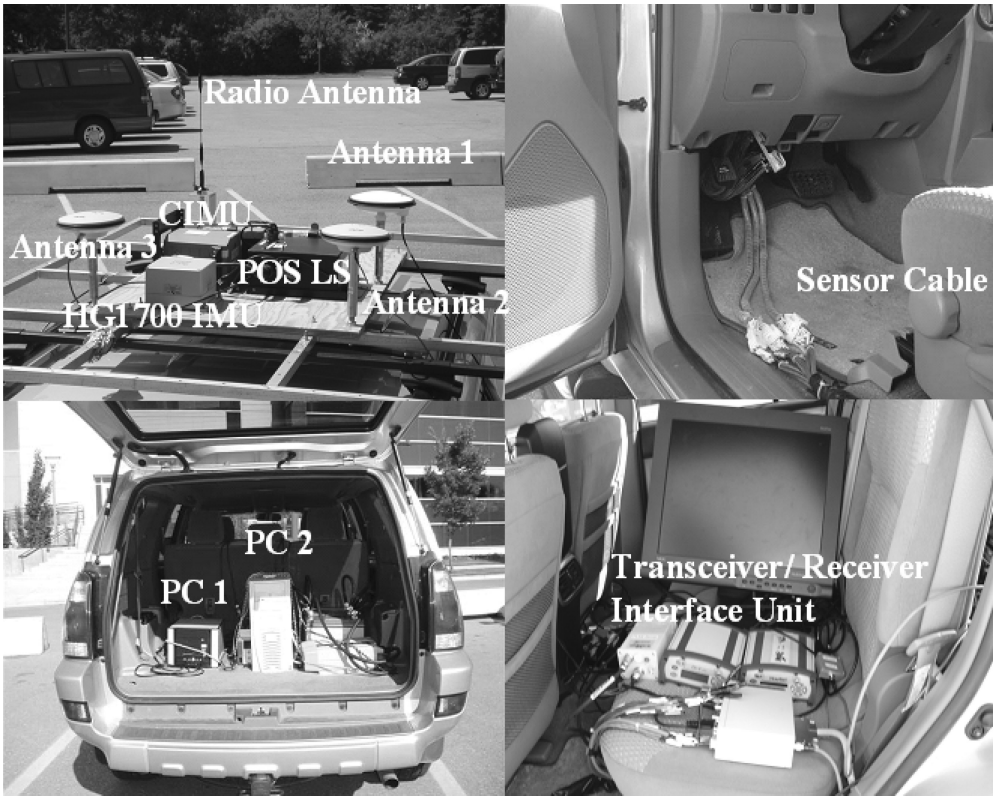

Figure 3 System Setup.

The MEMS IMU is of a much lower quality (gyro bias: >100 deg/h, accelerometer bias: >1.0 mg) and cost (<$2,000) than the tactical and navigation grade IMUs (Gao, 2007). To assess the performance of the GPS/MEMS IMU/SAS integrated system, a reference solution is generated from another independent system such as the GPS/HG1700 IMU (tactical-grade IMU) integrated system or GPS/CIMU (navigation-grade IMU). As shown in the hardware platform description in Figure 3, three different GPS units are employed to integrate with navigation-grade, tactical-grade and MEMS IMUs for generating independent solutions. Through a connection between the sensor cable and the interface unit, the on-board vehicle sensors and the MEMS IMU data are time-tagged and logged onto the PC1 via a serial port. Radio link antennas and transceivers were used to broadcast the GPS reference station data for the real-time test. The CIMU data was collected by an Applanix POS LS system. The open-sky test has a good GPS availability. Its reference solution is generated by the GPS/tactical-grade HG1700 IMU integrated system. In the real-time tests, however, partial and complete GPS outages are mainly introduced by dense foliage, small buildings near the street as well as bridges, and the GPS/navigation-grade CIMU is, therefore, needed to generate the reference solution.

The purpose of the open-sky test processed in post-mission is to test the software for tuning of the Kalman filter and modeling of the sensors. Figure 4 gives an overview of the test environment. With a maximum GPS baseline length of 4 km as well as an ideal environment for GPS ambiguity resolution, the GPS measurements used in this test included L1 carrier phase, Doppler, and the C/A pseudorange.

The real-time tests conducted in suburban and pseudo-urban areas gave an evaluation of the validity of the design of the Kalman filter as well as the impact of the integration of the steering angle sensor when the satellite signals were masked.

The real-time test in a suburban area was conducted with a maximum baseline of 2.5 km. As shown in Figure 5, the GPS reference station and radio link antennas were set up on the roof of the CCIT building at the University of Calgary. Also, partial and complete GPS outages were mainly introduced by the dense foliage, small buildings near the street, as well as bridges. Unlike the open-sky area, the multipath error significantly increased in suburban or pseudo-urban areas. To guarantee reliable ambiguity resolution, the widelane (L1-L2) carrier phase (rather than L1 in the open-sky test), Doppler, and the C/A code pseudorange measurements were used.

Using the same GPS reference station as in the suburban area test, the pseudourban area test was conducted on the campus of the University of Calgary. The maximum baseline length was around 1 km. Multipath was more severe than that in the open-sky and suburban areas. Consequently, partial and complete GPS masking was more frequently encountered in the pseudo-urban area test because of the tall buildings, trees, and underpasses. The masking duration was also longer than in the suburban area; therefore, the widelane carrier phase, Doppler and C/A code

Figure 4 Open-sky Test Processed in Postmission.

pseudorange measurements were also used. Figure 6 shows the environment for the pseudourban area test. The position drift errors were measured by comparing the integration strategy for the GPS/MEMES IMU and GPS/MEMS IMU/SAS systems with the GPS/CIMU integrated reference solution. Even though the navigation-grade CIMU also drifts with time without GPS aiding, it drifts to a much smaller degree than the MEMS IMU due to its high accuracy (decimeter level) and good quality (Gao, 2007).

Figure 7 shows the actual position differences between the reference solution and the GPS/MEMS IMU/SAS integrated with the corresponding 3-sigma envelope of the estimated standard deviations when GPS is fully available. It can be seen that the difference is at the centimeter level. Consequently, GPS plays

Figure 5 Real-time Test in a Suburban Area.

Figure 6 Real-time Test in Pseudo-urban Area.

a dominant role and determines the system positioning accuracy in this case. As expected, most of the differences are within the 3-sigma boundary. The consistency of the actual differences and the estimated standard deviations of the differences indicate that the Kalman filters are well tuned for this scenario.

For the open-sky test processed in postmission, the system performance and positioning accuracy for integration of the steering angle sensor are assessed by simulating GPS outages over various time intervals. In total, 12 GPS outages were simulated each with a duration of 40 s.

To illustrate the position drift error for the 12 simulated 40-s GPS outages, and to analyze the validity of the Kalman filter, Figure 8 shows the RMS horizontal position error across all outages and the average estimated standard deviation (from the Kalman filter). The solid lines represent the RMS error, and the dashed lines represent the average estimated deviation. The estimated position standard deviations in the Kalman filter are estimates of the errors from the Kalman filter, which should have good agreement with the actual errors in an ideal case. In practice, however, it indicates that the model and parameters in the Kalman filter are well tuned if the estimated standard deviation does not deviate too much from the variation of the actual error, or, more specifically, the position differences in this case.

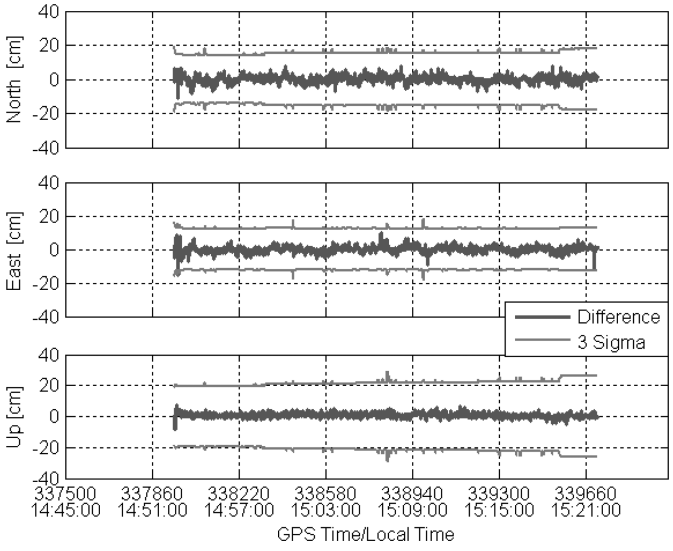

Figure 7 Position Differences Between GPS/MEMS IMU/SAS and the Reference for the Open-sky Test.

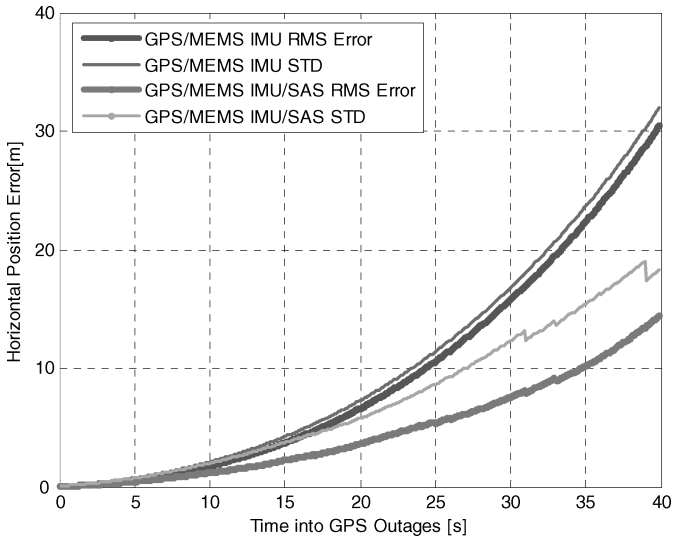

Figure 8 Horizontal Position Error and Average Estimated Standard Deviation with GPS Outages.

Table 1 Horizontal RMS position error and average estimated standard deviation at the end of 40-s GPS outages

Strategies	Horizontal RMS position error (m)	Horizontal average estimated standard deviation (m)
GPS/MEMS IMU	30.48	31.98
GPS/MEMS IMU/SAS	14.38	19.59

Table 2 RMS horizontal position error of real-time tests

Strategies	Suburban area (m)	Pseudourban area (m)
GPS/MEMS IMU	1.09	2.60
GPS/MEMS IMU/SAS	0.76	1.76

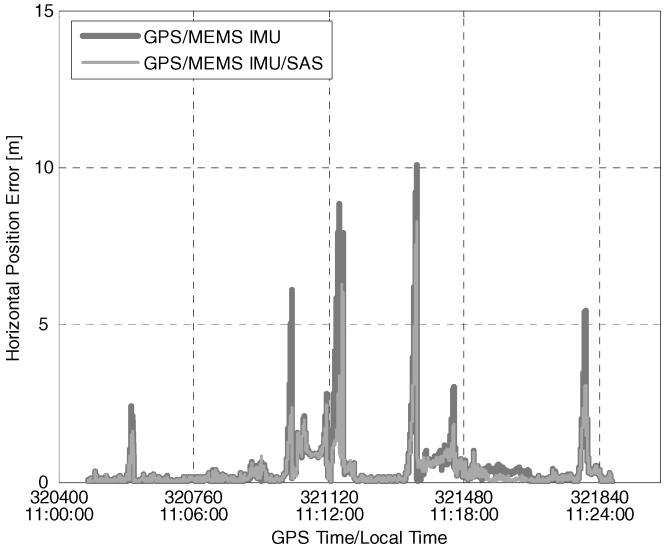

Figure 9 Horizontal Position Error for Suburban Area Real-time Test.

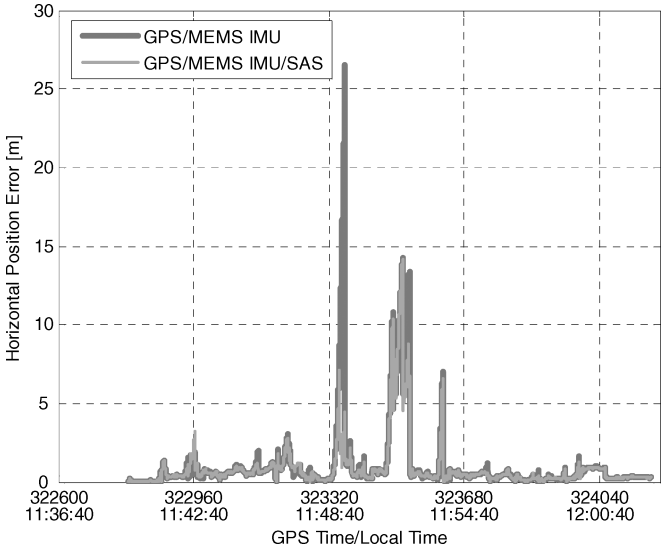

Figure 10 Horizontal Position Error for Pseudourban Area Real-time Test.

Table 1 summarizes the horizontal RMS position error and average estimated standard deviation at the end of the 40-s GPS outages. During the simulated GPS outages, the MEMS IMU standalone system drifts very rapidly. With an external aiding from the steering angle sensor, however, the horizontal positioning accuracy can be improved by about 53%. Furthermore, the actual horizontal position differences and the estimated standard deviations are consistent at an acceptable level, which indicates that the Kalman filter is well tuned.

For the real-time test in suburban area, the position computed from both the GPS/MEMS IMU and GPS/MEMS IMU/SAS integrated systems are compared with the reference solution. Figure 9 shows their horizontal position differences with respect to the GPS/CIMU integrated system. When GPS is fully available, the horizontal positioning differences for each integration strategy are very small, as expected. The larger horizontal position differences are correlated with GPS outages. The benefit gained from the steering angle sensor on the standalone MEMS IMU is a reduction in the horizontal position error. To be more specific, the horizontal position difference shown at epochs 321120 s and 321320 s can be reduced from approximately 8–10 m with the stand-alone MEMS IMU to approximately 6–7 m by integrating the steering angle sensor with the MEMS IMU. Table 2 summarizes the RMS horizontal position error over the entire time period of the real-time test. Compared to the GPS/MEMS IMU integrated system, the percentage improvements for the horizontal positioning accuracy from the steering angle sensor is 30% for the suburban area real-time test.

Similar to the analysis in the suburban area test, Figure 10 shows the position errors of the GPS/MEMS IMU and GPS/MEMS IMU/SAS systems. Compared to the suburban area test, the position drift errors are larger (maximum of approximately 26 m in the horizontal direction) for the MEMS IMU standalone system without any external aiding from GPS and steering angle sensor. This is due to the more frequent and much longer duration of the GPS outages occurring in the pseudourban area; however, the positioning accuracy can be enhanced by 32% with the integration of the steering angle sensor over the entire test period, as shown Table 2 for the RMS horizontal position errors in the real-time tests.

CONCLUSIONS

The objective of the article is to enhance positioning accuracy during GPS outages. With a centralized Kalman filter, the steering angle sensor is tightly coupled with GPS and a MEMS IMU. The integration algorithm indicates that the steering angle can be observed from the velocity in kinematic mode. As an external aiding on MEMS IMU, the steering angle sensor can provide a constraint on velocity; therefore, the integration of the steering angle sensor can enhance the horizontal positioning accuracy during GPS outages.

Compared to the GPS/MEMS IMU integrated system, the percentage improvement in the horizontal positioning accuracy from the steering angle sensor are 53% for the open-sky test (postmission processing with 12 simulated GPS outages), 30% for suburban area real-time test, and 32% for pseudourban area real-time test.

REFERENCES

Bevly, D. M. (2001). High speed, dead reckoning, and towed implement control for automatically steered farm tractors using GPS, Ph.D. thesis, Stanford University.

Bonnifait, P. H. (2003). Fusion of redundant ABS sensors. *The Journal of Navigation, The Royal Institute of Navigation*, **56**, 429–441.

Carlson, C. R. (2003) Estimation with applications for automobile dead reckoning and control, Ph.D. thesis, Stanford University.

Dissanayake, G., Sukkarieh, S., Nebot, E., and DurrantWhyte, H. (2001). The aiding of a low cost strapdown inertial measurement unit using vehicle model constraints for land vehicle applications. *IEEE Transactions on Robotics and Automation*, **17**(5), 731–747.

Gao, J. (2007). Development of a precise GPS/INS/on-board vehicle sensors integrated vehicular positioning system, Ph.D. thesis, University of Calgary, (available at http://www.geomatics.ucalgary.ca/research/publications/GradTheses.html).

Godha, S. (2006). Performance evaluation of low cost MEMS-based IMU integrated with GPS for land vehicle navigation application, M.Sc. thesis, University of Calgary (available at http://www.geomatics.ucalgary.ca/research/publications /GradTheses.html).

Harvey, R. S. (1998). Development of a precision pointing system using an integrated multisensor approach, M.Sc. thesis, University of Calgary.

Hay, C. (2005). Turn, turn, turn wheel-speed dead reckoning for vehicle navigation. *GPS World*, **10**, 37–42.

Kubo, J., Kindo, T., Ito, A., and Sugimoto, S. (1999). DGPS/INS/wheel sensor integration for high accuracy land-vehicle positioning, Proceedings of ION GPS 1999, Institute of Navigation, Nashville, TN, 555–564.

Petovello, M. G. (2003). Real-time integration of tactical grade IMU and GPS for high-accuracy positioning and navigation, PhD thesis, University of Calgary, (available at http://www.geomatics.ucalgary.ca/research/publications/GradTheses.html).

Stephen, J. (2000). Development of a multisensor GNSS-based navigation system, M.Sc. thesis, University of Calgary, (available at http://www.geomatics.ucalgary.ca/research/publications/GradTheses.html).

Teunissen, P. J. G., and Kleusberg, A. (1996). GPS for Geodesy. New York: Springer.